Dip-Sequence Analysis

9.1 Introduction

The three-dimensional geometry of a structure can be determined from the bedding attitudes measured in a single well bore or on a traverse through a structure. The method of dip sequence analysis presented here was developed for the structural analysis of dipmeter logs by Bengtson (1981a) but is equally informative whether the traverse is down a well or along a stream. Major problems with the structural interpretation of dip data are the high stratigraphic noise content and the complexity of the structures to be interpreted. Dip sequence analysis techniques, called Statistical Curvature Analysis Techniques (SCAT or SCAT analysis) by Bengtson (1981a), are particularly good for extracting the structural signal from the noise. Using SCAT it is possible to determine the plunge of folds, the locations of fold axial surfaces, crests, and troughs, to infer the strike and dip directions of faults, and to separate regional fold trends from local fault trends. The power of the technique derives from (1) the noise-reduction strategy of examining the data as dip components in both the strike and dip directions of folding and (2) providing models for the SCAT responses of the geometry to be interpreted.

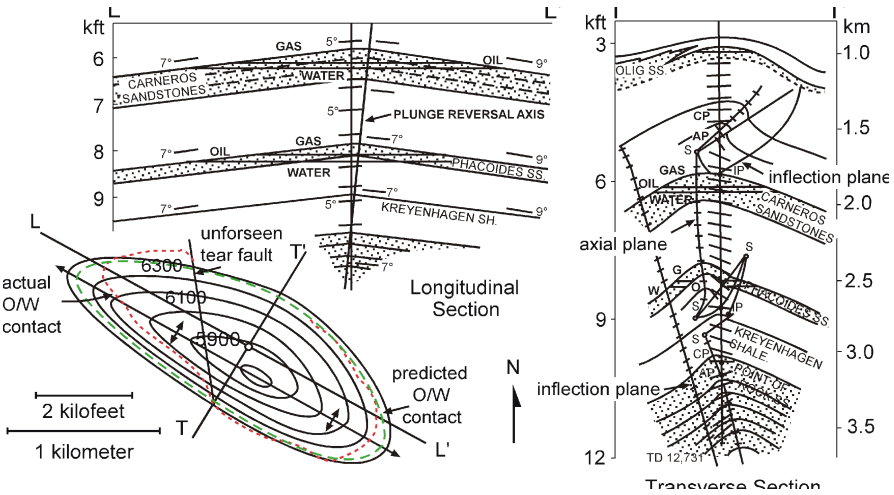

Fig. 9.1. Railroad Gap Field, California, predicted longitudinal and transverse cross sections and structure contour map on the top Carneros sandstone, based on the SCAT analysis of a single well at the crest of the anticline. *O/W:* oil-water contact. (After Bengtson 1981a)

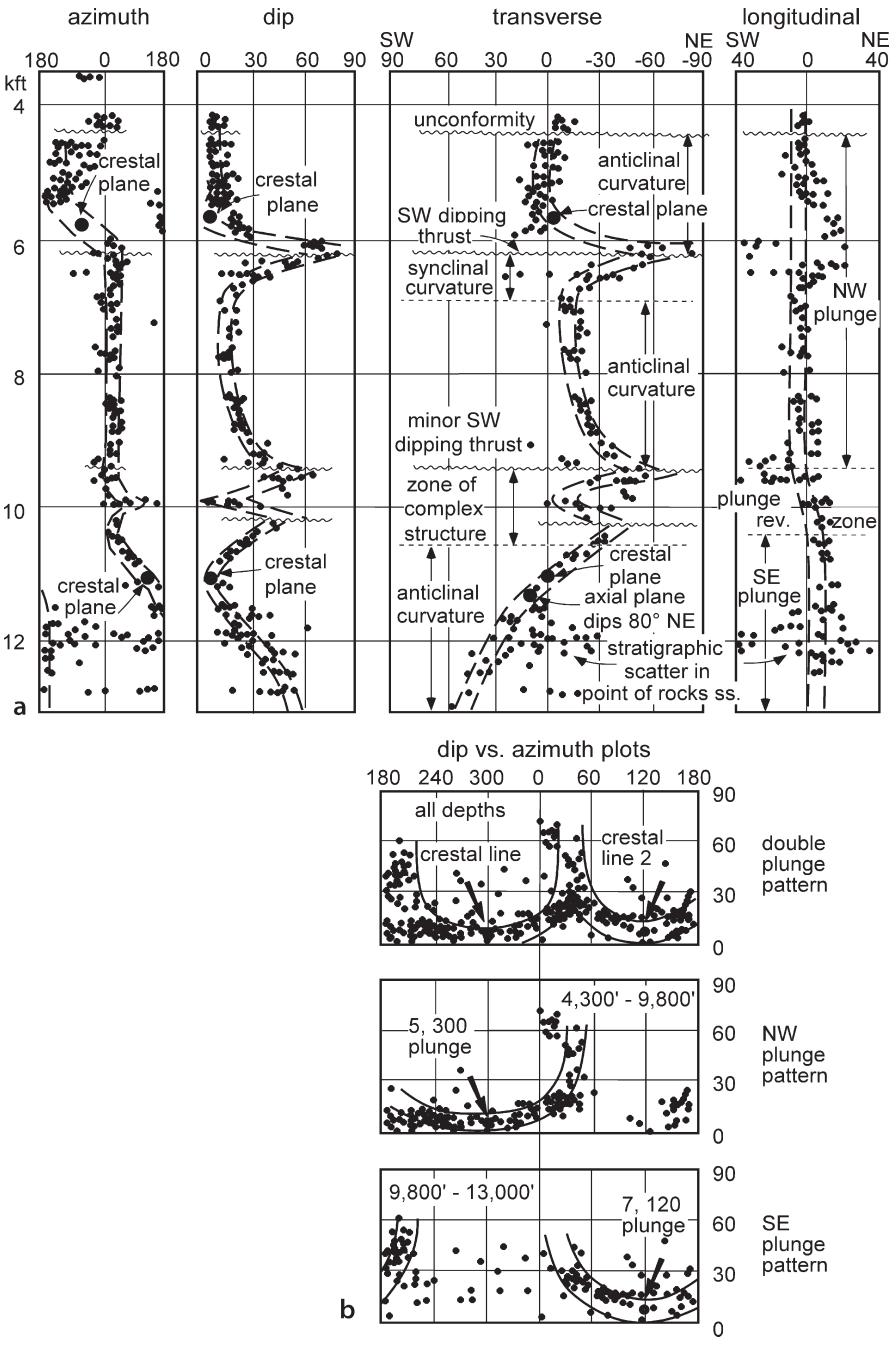

Fig. 9.2. SCAT plots for the discovery well of Railroad Gap Field, California. For the map and cross sections see Fig. 9.1. **a** Dip component vs. depth plots. **b** Dip vs. azimuth plots. (After Bengtson 1981a)

The potential of the method is indicated by the interpretation of the Railroad Gap oil field on the basis of the SCAT analysis of a single, favorably located well (Figs. 9.1, 9.2). SCAT analysis (Bengtson 1981a) was used to predict the structure on perpendicular cross sections from which the map was generated. The map view shows the close correspondence between the predicted and observed oil-water contact.

9.2 Curvature Models

Figure 9.3 illustrates the basic curvature geometries. The first step in the analysis is to differentiate a monoclinal dip sequence from a fold. This is accomplished with an azimuth histogram and/or with a tangent diagram. An azimuth histogram is a plot of the azimuth of the dip versus the amount of the dip (Fig. 9.4). The natural variation of

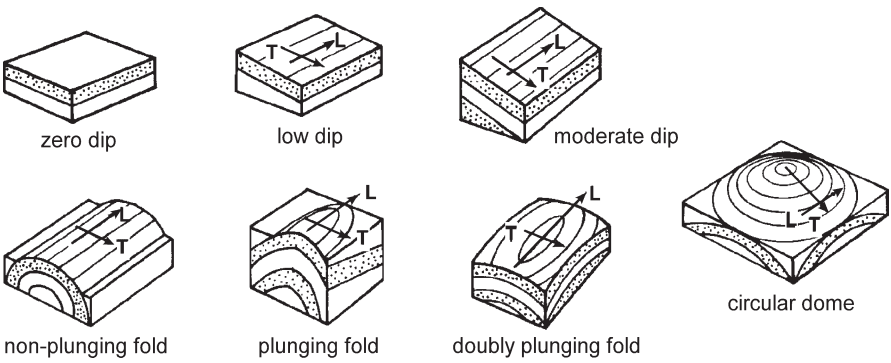

Fig. 9.3. Models of structural curvature geometries. *L:* Longitudinal; *T:* transverse. (Bengtson 1981a)

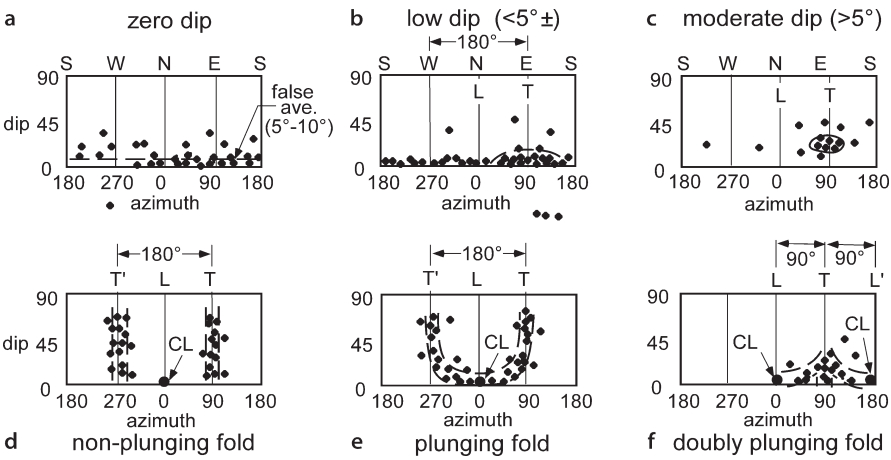

Fig. 9.4. Dip vs. azimuth patterns corresponding to the models of Fig. 9.3. *CL:* crestal line (after Bengtson 1981a). **a** Zero dip. **b** Low dip. **c** Moderate dip. **d** Non-plunging fold. **e** Plunging fold. **f** Doubly plunging fold

dips around a monoclinal dip gives a horizontal distribution of noise. Thus a zero true dip gives a small false positive average on the azimuth histogram because all dips are recorded as positive (Fig. 9.4a). As the dip increases the dips form point concentrations that become better defined as the true dip increases (Fig. 9.4b,c). Non-plunging and uniformly plunging folds give vertical concentrations of points corresponding to the limbs (Fig. 9.4d,e) and a doubly plunging fold produces an arrow-head-shaped distribution of points (Fig. 9.4f). On a tangent diagram a monocline plots as a point concentration of dips, and a fold (Figs. 5.3, 5.5) will produce a linear or curvilinear concentration of points.

9.3 Dip Components

A key step in a SCAT analysis is to determine the dip components in the transverse direction (T = transverse = regional dip) and the longitudinal direction (L = longitudinal = regional strike) which is at right angles to it. These dip components represent the dips on vertical cross sections in the T and L directions and are used to produce the SCAT histograms (Fig. 9.2) and cross sections (Fig. 9.1) in the T and L directions. The T and L directions are found from the dip vs. azimuth histogram (Fig. 9.4) or from the plot of bedding dips on a tangent diagram (Fig. 9.5). For monoclinal dip, the center of the point concentration on the dip-azimuth histogram is the T direction and the L direction is 90° away from it (Fig. 9.4b,c). For a fold, the center of the limb concentrations on an azimuth histogram is the T direction and the midpoint between the concentrations is the L direction (Fig. 9.4d–f). On a tangent diagram (Fig. 9.5), the orientation of the crest (or trough) line is the L direction and the T direction is at right angles to the crest (or trough) line. Both the T and L lines go through the center of the tangent diagram regardless of the fold plunge.

The dip components can be found either graphically or analytically. In the graphical method, the T and L lines are drawn on a tangent diagram. The T and L components are the projections of the dip vectors onto the T and L axes (Fig. 9.6). The dip com-

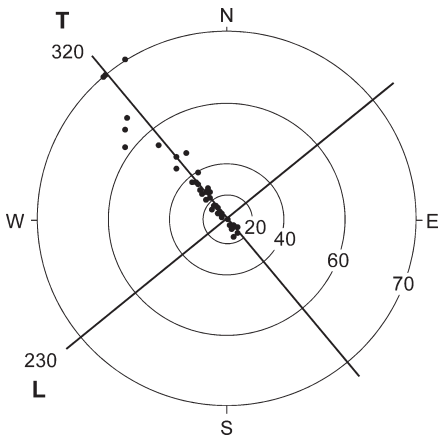

Fig. 9.5. Determination of T and L directions on the tangent diagram of a fold. *Solid dots* represent dip vectors of bedding

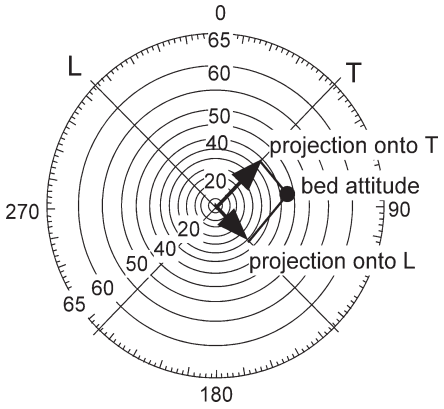

Fig. 9.6.
Dip components in *T* and *L* directions. Here the *T* direction is NE–SW and the *L* direction is NW–SE. Bed attitude is 55, 082. The dip components are the lengths found by orthogonal projection of the dip vector onto the *T* and *L* lines. The *T* component is 50°NE and the *L* component is 40°SE

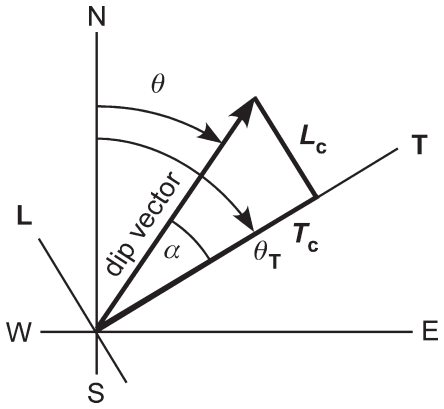

Fig. 9.7.
Geometry of the *T* and *L* components. α: angle between dip vector and *T* direction; θ_T: azimuth of *T* direction; θ: azimuth of dip vector; T_c: *T* component; L_c: *L* component

ponents are themselves vectors and have both magnitude and direction. The quadrant of the component, as well as its magnitude, must be recorded.

The dip components can easily be found analytically. Based on the geometry of Fig. 9.7,

$$\alpha = \theta_T - \theta \quad , \tag{9.1}$$

$$T_c = \delta \cos \alpha \quad , \tag{9.2}$$

$$L_c = \delta \sin \alpha \quad , \tag{9.3}$$

where $T_c = T$ component, $L_c = L$ component, α = angle between dip vector and *T* direction, θ_T = azimuth of *T* direction, θ = azimuth of dip vector, δ = dip. Computer programs for the preparation of SCAT diagrams have been published by Elphick (1988). SCAT analysis can be performed entirely on a spreadsheet. Plot the tangent diagram as described in Sect. 2.8, use Eqs. 9.1–9.3 to find the *T* and *L* components, and plot the dip-component diagrams as *xy* graphs.

9.4 Analysis of Uniform Dip

The dip component diagrams are the primary noise reduction strategy in SCAT analysis. For zero dip the azimuth of the dip is random (actually stratigraphic scatter) and the dip amount shows a false positive average (Fig. 9.8). As the amount of homoclinal dip increases (Figs. 9.9, 9.10) the concentration of points becomes sharper. The component plots for zero dip show the correct zero average (Fig. 9.8). Low and moderate planar dips (Figs. 9.9, 9.10) show their true dip values on the transverse component plots because these are in the dip direction. The longitudinal dip components average zero because they are in the strike direction. The zero *L* component average (Figs. 9.9, 9.10) confirms the choice of the *L* and *T* directions.

9.5 Analysis of Folds

Folds produce distinctive curves on the dip vs. depth plots. The azimuth vs. depth plot shows the reversal of azimuth at the crest of the fold, CP (Figs. 9.11–9.13). The dip component plots are the most informative. The transverse component plots all cross the zero dip line at the crest of the anticline (CP), show an inflection point at the axial plane (AP) and show a dip maximum at the inflection plane (IP) that separates anticlinal curvature from synclinal curvature. Any variations in plunge are apparent on the longitudinal component plot. The non-plunging fold (Fig. 9.11) is defined by a straight line on the plot of

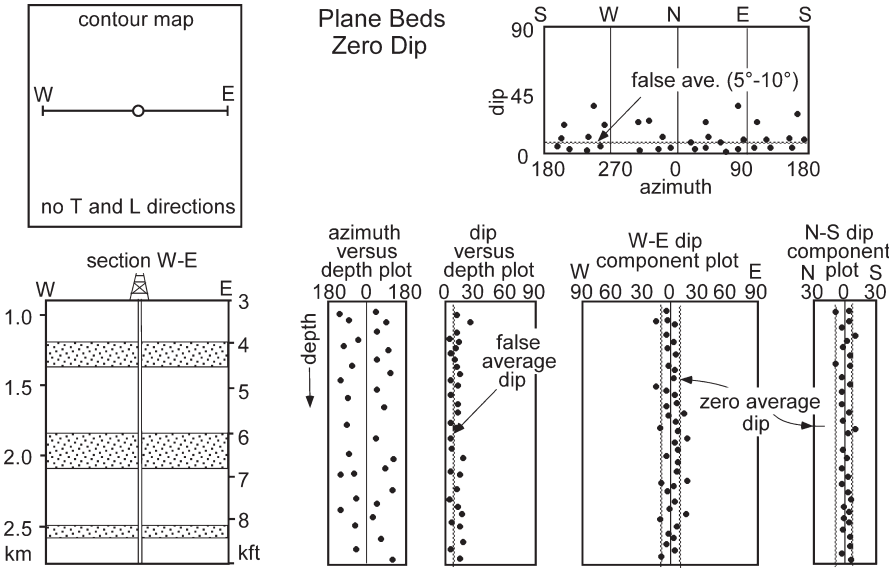

Fig. 9.8. Model map, cross section and SCAT plots for zero dip. (After Bengtson 1981a)

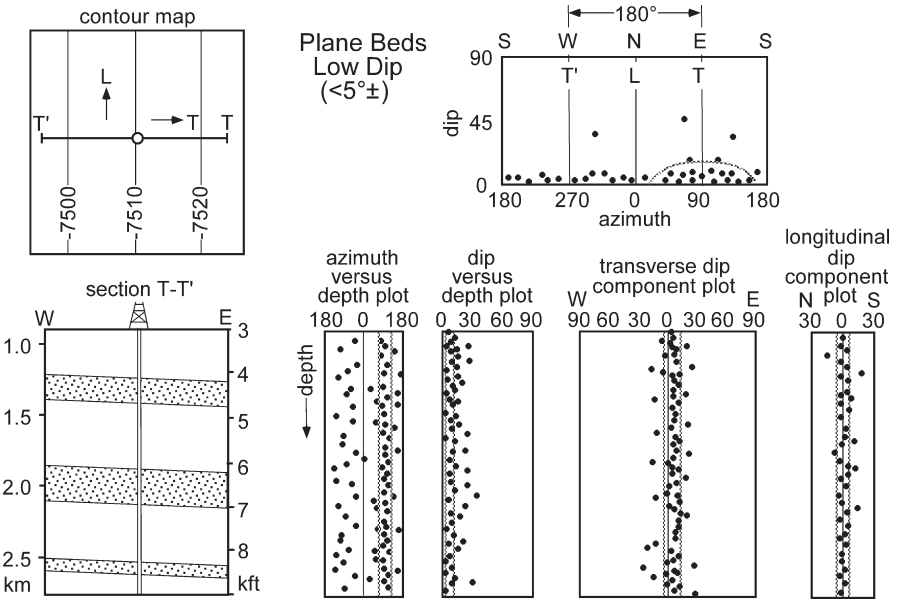

Fig. 9.9. Model map, cross section and SCAT plots for low monoclinal dip. (After Bengtson 1981a)

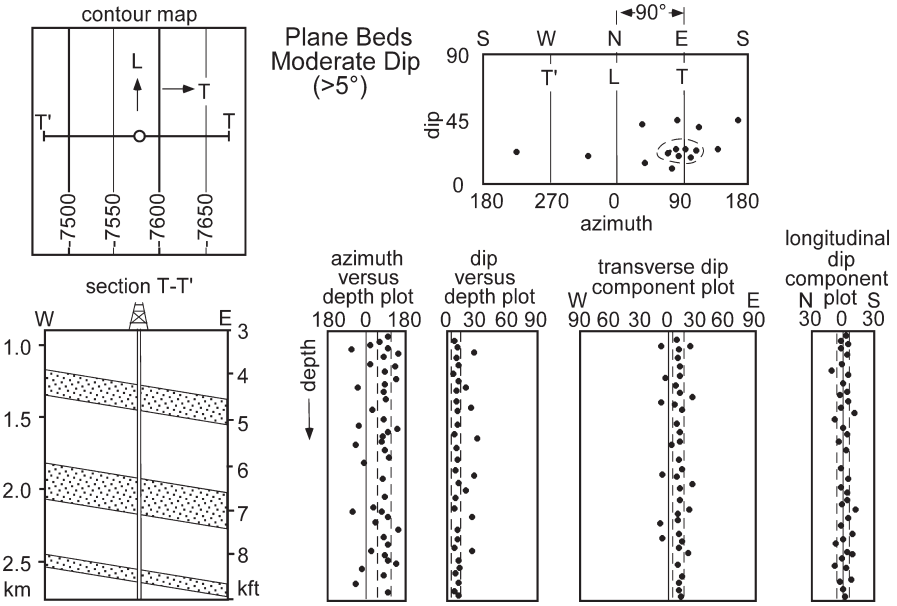

Fig. 9.10. Model map, cross section and SCAT plots for moderate to steep monoclinal dip. (After Bengtson 1981a)

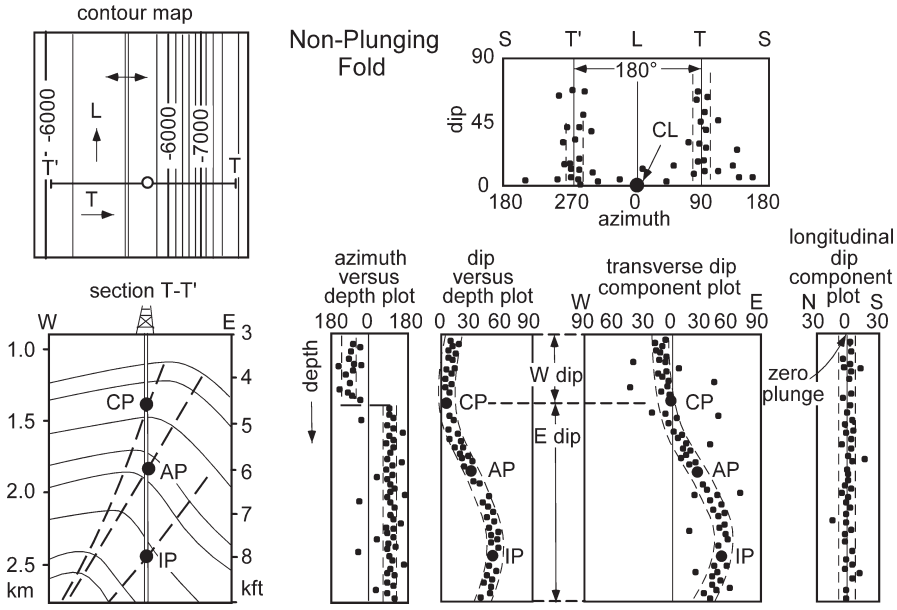

Fig. 9.11. Model map, cross section and SCAT plots for a non-plunging fold. *AP:* axial plane; *CL:* crestal line; *CP:* crestal plane; *IP:* inflection plane. (After Bengtson 1981a)

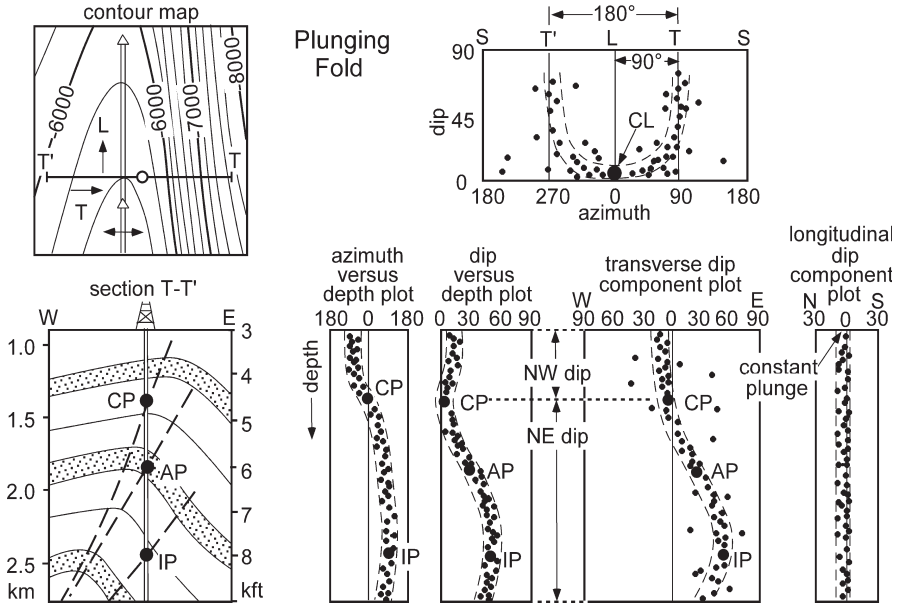

Fig. 9.12. Model map, cross section and SCAT plots for a plunging fold. *AP:* axial plane; *CL:* crestal line; *CP:* crestal plane; *IP:* inflection plane. (After Bengtson 1981a)

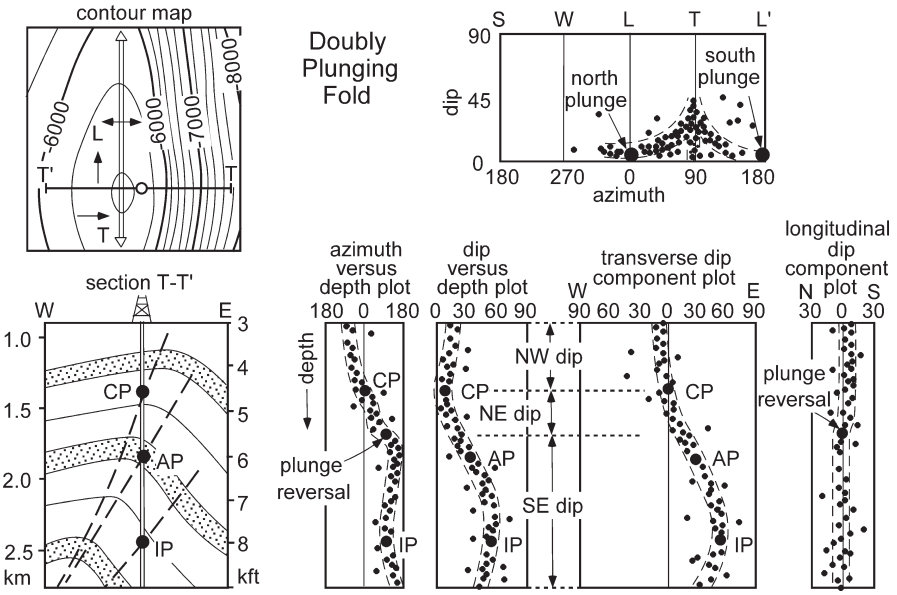

Fig. 9.13. Model map, cross section and SCAT plots for a doubly plunging fold. *AP:* axial plane; *CP:* crestal plane; *IP:* inflection plane. (After Bengtson 1981a)

L dip with depth that gives the average plunge of zero. A uniformly plunging fold (Fig. 9.12) plots as a line of constant plunge with depth. A doubly plunging fold (Fig. 9.13) shows the plunge reversal with depth on the *L* component plot.

Dip-sequence analysis can be performed on a traverse in any direction through a structure. As an example, the method is applied to a horizontal traverse across the map of the Sequatchie anticline originally presented in Fig. 2.4. The traverse (Fig. 9.14) runs from northwest to southeast at right angles to the fold axis along a stream valley that provides the best exposure and therefore the most data. The traverse is broken into three straight-line segments at the dashed lines in order to follow the valley. The attitudes of bedding are located on the SCAT diagrams according to their distance from the northwest end of the traverse. The numerical values are given in Table 9.1.

The *T* and *L* directions are determined from the tangent diagram and the dip-azimuth diagram. The linear trend of dips on the tangent diagram (Fig. 9.15a) is the trend of *T*, and *L* is at right angles to it. On the dip-azimuth diagram (Fig. 9.15b) the two vertical lines of points indicate, by comparison to Fig. 9.4, a non-plunging fold with a crest that trends 230. The dip-azimuth diagram should always be checked against the tangent diagram before finally deciding on the plunge direction and amount. Here the trend of the crest and the lack of significant plunge agrees with the tangent diagram. The direction of the crest line, here equal to the fold axis direction, is the *L* direction to be used in the next stage of the analysis. The *T* direction is at 90° to *L*, parallel to the azimuth of the limb dip.

The SCAT diagrams reveal the details of the structure. The bedding azimuths and dip components are plotted in Fig. 9.16. The azimuth and dip diagrams (Fig. 9.16a,b) show the locations of the crestal plane, axial plane, and inflection plane (compare

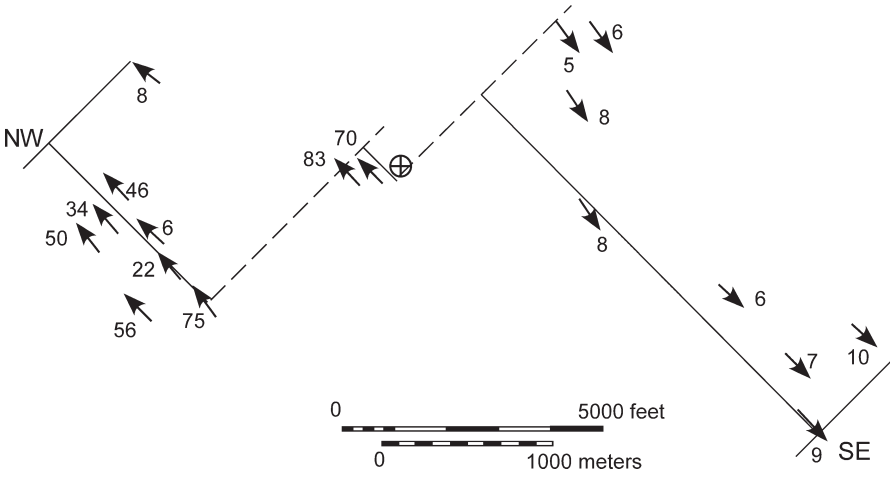

Fig. 9.14. Dip traverse across the Sequatchie anticline in the Blount Springs area, showing locations of bedding attitude measurements. *Dashed lines* are offsets in the line of traverse

Table 9.1.
Dip traverse across Sequatchie anticline

Distance from NW end of traverse (ft)	Dip, azimuth	T component (from 320/140)	L component (from 230/50)
256	8, 308	8 NW	1 SW
1 384	46, 315	45 NW	7 SW
1 640	34, 316	34 NW	2 SW
1 660	50, 320	50 NW	0
2 328	6, 320	6 NW	0
3 143	22, 316	22 NW	1 SW
3 261	56, 318	56 NW	1 SW
4 096	75, 330	75 NW	25 SW
4 253	Break		
4 253	83, 315	83 NW	~45 SW
4 528	70, 315	70 NW	13 SW
4 891	0, 000	0	0
5 147	Break		
5 323	5, 145	5 SE	1 SW
5 815	6, 144	6 SE	1 SW
6 404	8, 145	8 SE	1 SW
8 005	8, 144	8 SE	1 SW
10 942	6, 127	6 SE	1 NE
12 789	7, 136	7 SE	1 NE
13 466	10, 136	10 SE	1 NE
13 692	9, 136	9 SE	1 NE

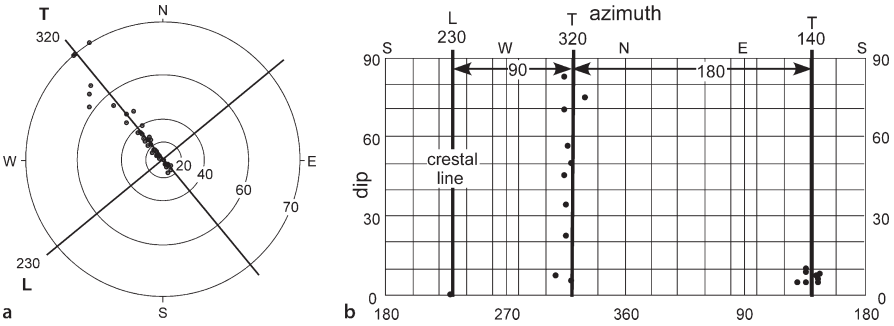

Fig. 9.15. Finding the *T* and *L* directions for the traverse across the Sequatchie anticline. **a** Tangent diagram. **b** Azimuth-dip diagram. *T* transverse dip direction; *L* longitudinal dip direction; crest line is at 0, 230

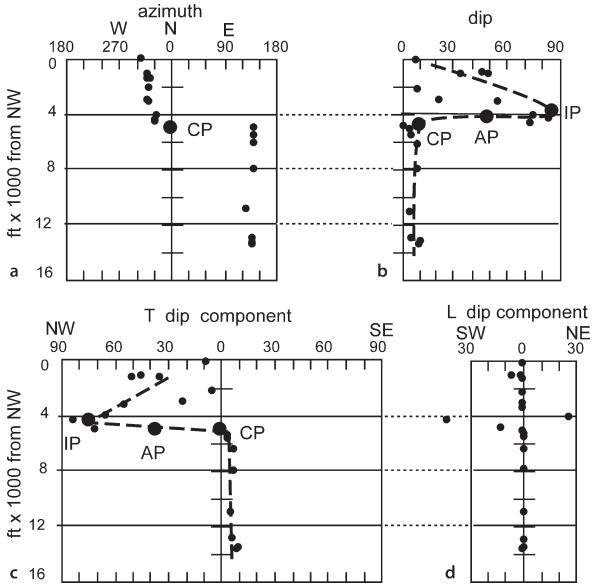

Fig. 9.16.
SCAT analysis of the Sequatchie anticline. **a** Azimuth-distance diagram. **b** Dip-distance diagram. **c** *T* component dip-distance diagram. **d** *L* component dip-distance diagram. *AP:* axial plane; *CP:* crestal plane; *IP:* inflection plane

Fig. 9.16 with 9.11). The locations of the crestal plane and inflection plane are well defined in Fig. 9.16b,c and the axial plane falls between the two. Note that in the dip-depth (distance) plot (Fig. 9.16b) all dips plot to the right, whereas in the *T*-component plot the dips are plotted by their quadrant direction. The dip data for the northwest limb is noisy, even on the *T*-component plot, although the signal remains clear. Most of the dips on the *L*-component diagram (Fig. 9.16d) are zero or close to zero, confirming the choice of the plunge direction and the interpretation that the plunge is zero. Significant plunge aberrations occur between the inflection plane and the crest plane which is the location of the steep limb of the structure. This suggests that the structure of the steep limb is complex, perhaps containing obliquely plunging minor folds, not just a simple monoclinal dip or curvature around a single axis.

9.6 Analysis of Faults

The drag geometry (Sect. 7.2.7) provides the basis for fault recognition by SCAT analysis. The presence of a fault is recognized from the distinctive cusp pattern on the transverse dip component plot (Figs. 9.17–9.20). A cusp is also present on the dip vs. depth plot but may not be as clearly formed. The cusp is caused by the dips in the drag fold adjacent to the fault and is expected to occur within a distance of meters to tens of meters from the fault cut. A traverse perpendicular to the fault plane will show the minimum affected width, whereas a traverse at a low angle to the fault plane, such as a vertical well drilled through a normal fault, will show the maximum width. The fault cut is at the depth indicated by the point of the cusp. The azimuth vs. depth plots distinguish between steepening drag that occurs where the faults dip in the direction of the regional dip of bedding (Fig. 9.17) and flattening drag that occurs where the fault dip is opposite to the regional dip of bedding (Fig. 9.18). Steepening drag maintains a constant dip direction whereas flattening drag may produce a reversal in the dip direction. A drag-fold axis that is oblique to the regional fold axis produces multiple fold axes on the dip-azimuth diagram (Figs. 9.19, 9.20). Both the regional dip and the drag-fold axis appear on the dip-azimuth diagram and the tangent diagram, allowing both directions to be determined.

If either the dip direction of the fault or its sense of slip is known, the other property of the fault can be determined from the direction the cusp points on the *T*-component

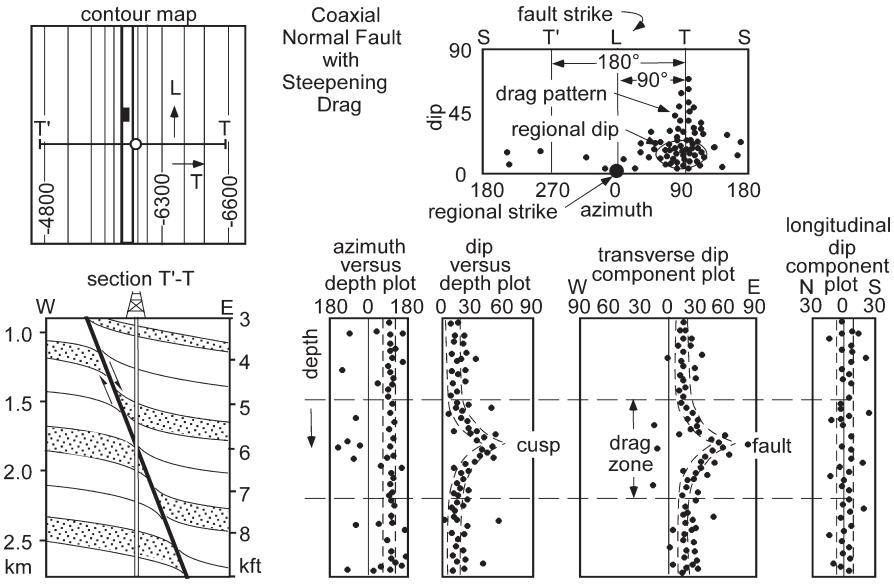

Fig. 9.17. Structure contour map, cross section, and SCAT plots for a normal fault with drag that steepens the regional dip. Fault strike is parallel to the regional strike. *L:* regional strike; *T:* regional down-dip direction; *T':* regional up-dip direction. (After Bengtson 1981a)

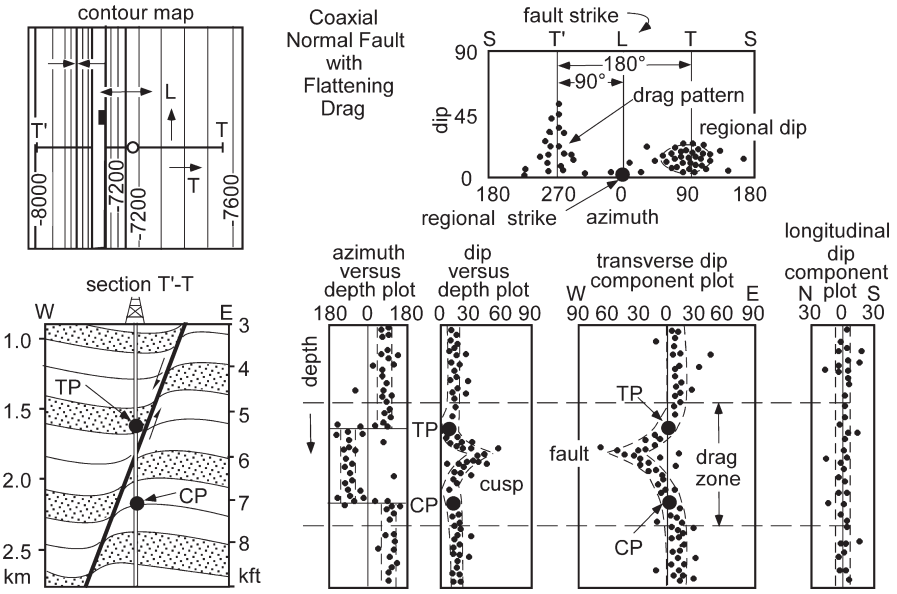

Fig. 9.18. Structure contour map, cross section, and SCAT plots for a normal fault whose drag flattens the regional dip. Fault strike is parallel to regional strike. *L:* regional strike; *T:* regional down-dip direction; *T':* regional up-dip direction; *CP:* crestal plane; *TP:* trough plane. (After Bengtson 1981a)

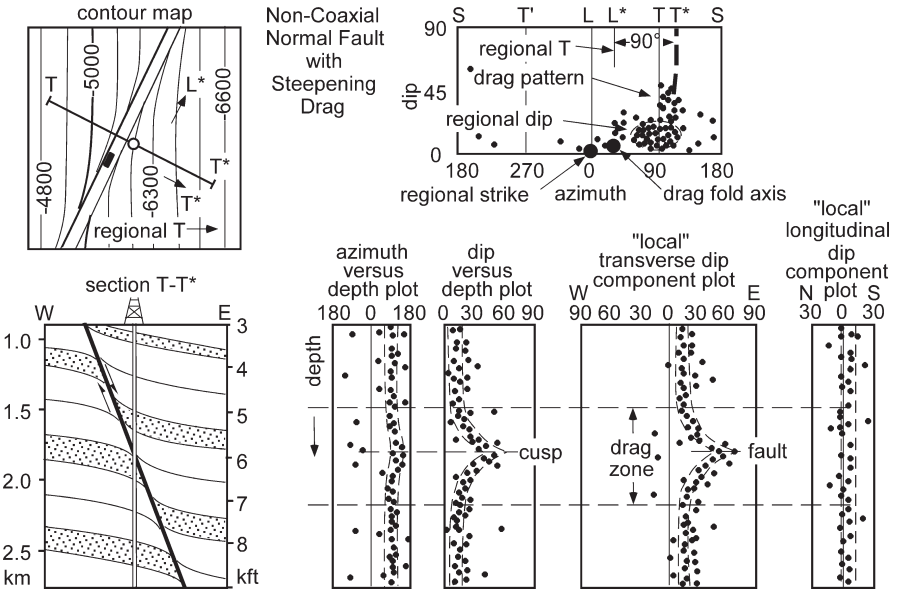

Fig. 9.19. Structure contour map, cross section, and SCAT plots for a normal fault striking oblique to regional dip with drag that steepens the regional dip. *L:* regional strike; *T:* regional down-dip direction; *T':* regional up-dip direction; *L*:* fault strike; *T*:* normal to fault strike. (After Bengtson 1981a)

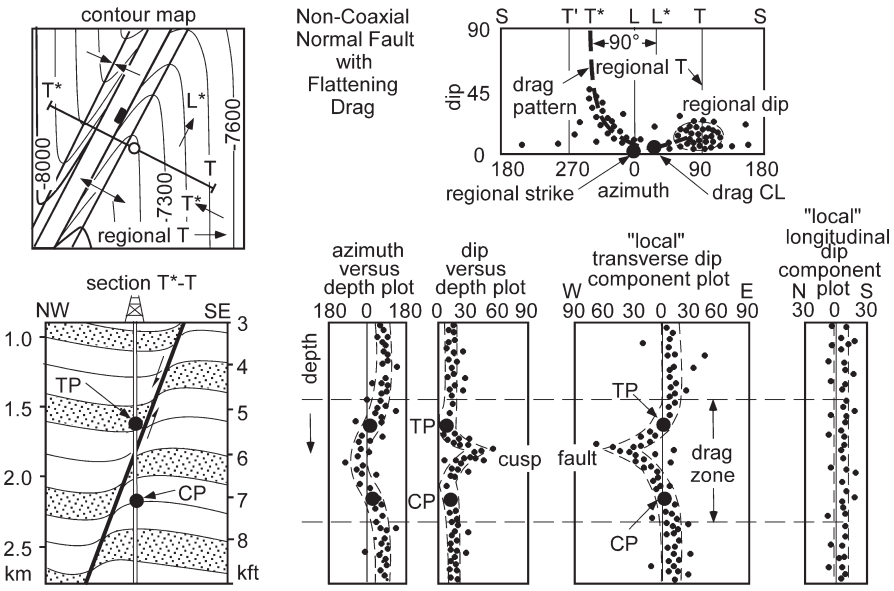

Fig. 9.20. Structure contour map, cross section, and SCAT plots for a normal fault striking oblique to regional dip with drag that flattens the regional dip. *L:* regional strike; *T:* regional down-dip direction; *T':* regional up-dip direction; *L*:* fault strike; *T*:* normal to fault strike; *CP:* crestal plane; *TP:* trough plane. (After Bengtson 1981a)

diagram. For a normal fault, the cusp points in the direction of the fault dip. For a reverse fault, the cusp points opposite to the direction of the fault dip. Note that the cusp on the dip vs. depth plot always points in the same direction because the dips are not plotted according to direction.

A drag fold may be present on one side of the fault but absent on the other, resulting in a half-cusp pattern. As indicated by Fig. 9.21a, this geometry may be present at the map scale as well as at the drag-fold scale. Folds of this type produce a half-cusp pattern on the transverse dip component plot (Fig. 9.21b). In association with a reverse-fault, the dips may increase to vertical and then become overturned. On the *T*-component plot (Fig. 9.21b), the half cusp curves smoothly to the left to a 90° dip, then reappears where dips are 90° to the right. The isolated group of dips near 90° on the right represents overturned beds, providing a method for recognizing overturning from the dip sequence alone.

A synthetic example of a dipmeter run across a normal fault will serve to illustrate the method. The example also illustrates SCAT analysis using a spreadsheet. The traditional paper-copy dipmeter (Fig. 9.22) is a graph of dip versus depth in a well. The "tadpole" heads indicate the amount of dip and the tails the direction of dip. Solid heads represent the best data and open heads the worst. In the case of a four-armed dipmeter a solid head represents a dip based on correlation of all four arms and an open head means three of the four arms can be correlated. If only two arms can be correlated, the dip cannot be calculated and no point is plotted. The numerical data set is given in Table 9.2.

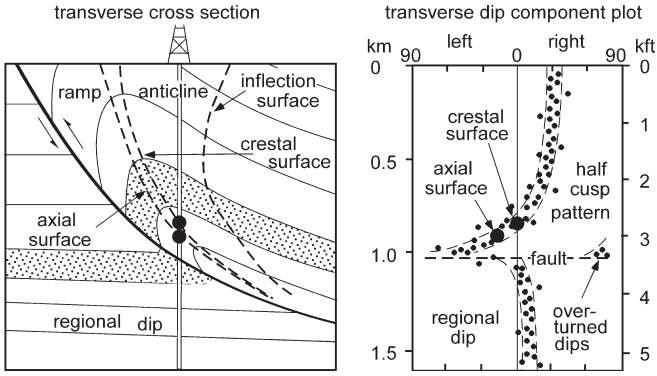

Fig. 9.21.
Drag geometry on a reverse fault showing a half-cusp transverse dip component plot and overturned beds. (After Bengtson 1981a)

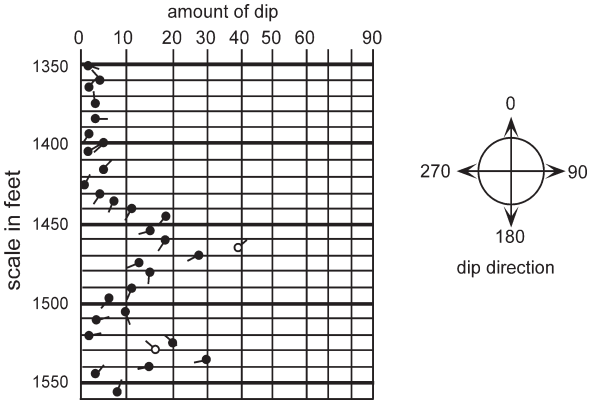

Fig. 9.22.
Synthetic dipmeter log representing a well containing a fault cut. Reference level for well is ground surface at 350 ft elevation. Quality ranking of data: *solid head:* best, *open head:* lower

Table 9.2.
Attitudes from dipmeter log in Fig. 9.22

Depth	Dip	Azimuth	Depth	Dip	Azimuth
–1350	2	115	–1465	39	46
–1360	4	320	–1470	27	242
–1365	2	41	–1475	13	250
–1375	3	350	–1480	15	190
–1385	3	91	–1490	11	204
–1395	2	206	–1495	6	219
–1400	5	227	–1505	10	155
–1405	2	66	–1510	4	72
–1415	6	45	–1520	2	79
–1425	1	29	–1525	20	322
–1430	5	213	–1530	16	314
–1435	7	200	–1535	30	259
–1440	11	212	–1540	15	260
–1445	18	223	–1545	4	42
–1455	15	258	–1555	8	24
–1460	18	209			

Interpretation begins with the azimuth-depth and dip-depth plots (Fig. 9.23). At shallower elevations in the well, the dip magnitude is consistently low and the azimuth highly variable. These are the characteristics expected for a low regional dip (c.f., Fig. 9.9). The next deeper interval appears to be a cusp on the dip-depth diagram. In the context of a cusp, the azimuth-depth diagram suggests flattening drag (c.f., Fig. 9.18). The lower portion of the well contains no clear structural pattern and may represent stratigraphic noise, perhaps a unit containing disparate dips like a conglomerate (where the pebble boundaries would produce dip readings) or a reef (where individual corals might be producing the dips).

Having isolated the cusp as an interval of interest, further analysis will be performed on that part of the well log alone. The *T* and *L* directions are most clearly found on the tangent diagram (Fig. 9.24a). There is a substantial amount of scatter but the least squares best-fit line does a good job of locating the *T* direction. Where it can be checked against other geological data, the best fit line has proved to be remarkably reliable, even where the scatter is large. If a quadratic best-fit line approximates a hyperbola and fits the data reasonably well, then the fold is probably conical. Where a quadratic best-fit is not hyperbolic, the best fit is linear and the fold is cylindrical. The dip-azimuth diagram (Fig. 9.24b) shows substantial scatter but can be interpreted with reference to Fig. 9.18 as showing a regional dip component and a drag-fold component. The results of this stage of the analysis give $T = 052$ and $L = 322$. Additional valuable information is the strike of the fault, which must be approximately parallel to the *L* direction, 322°.

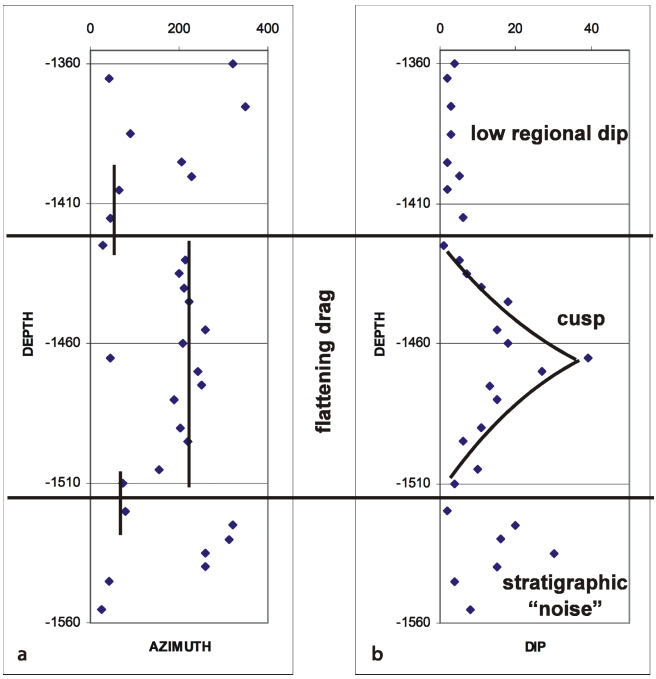

Fig. 9.23. Azimuth-depth and dip-depth diagrams for data in Table 9.2. **a** Azimuth versus depth. **b** Dip versus depth

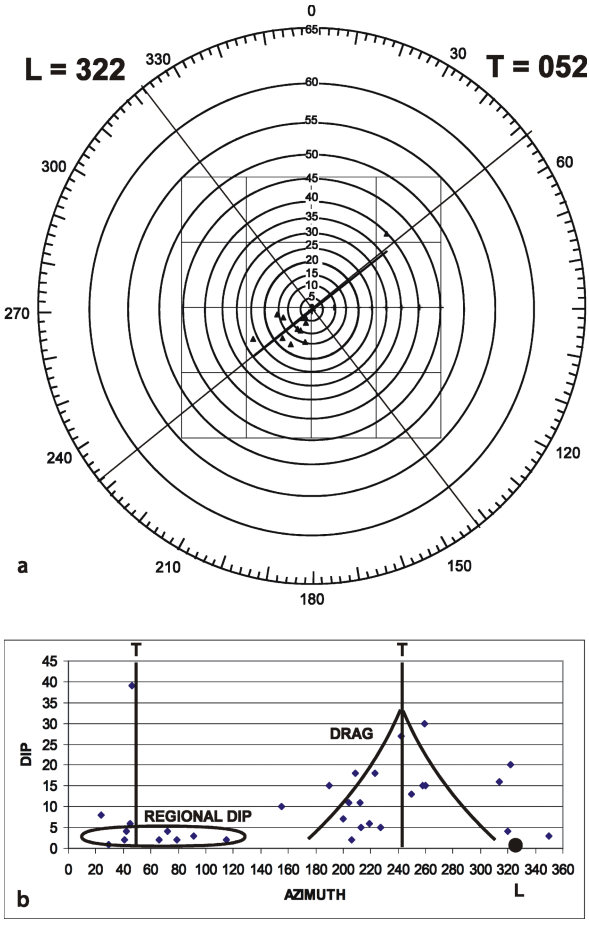

Fig. 9.24.
Determination of *T* and *L* directions for data in Table 9.2. **a** Tangent diagram. **b** Dip-azimuth diagram

The final part of the interpretation is based on the *T* and *L* component plots. A normal fault dips in the direction the cusp points on a *T* component plot, which is to the southwest for this example (Fig. 9.25a). At this stage, the effect of the choice of the *T* and *L* directions on the component plots should be examined. Vary their directions and watch for the effect on the *L*-component plot. The best result is one which shows the points falling the closest to the zero line, indicating that the *L* direction has been correctly chosen. The result in Fig. 9.25b is the best that can be obtained from this data set. Note that the data point that was at the tip of the cusp on the dip-depth plot (Fig. 9.23b) lies on the wrong (NE) side of the *T*-component plot (Fig. 9.25a). Re-examination of the original data (Fig. 9.22) shows this to be a point with poor data quality. It might represent a dip on a fracture or be a spurious result on fractured rock in the fault zone. No data at all might be expected from a fault zone in which the bedding has been highly disrupted by the deformation.

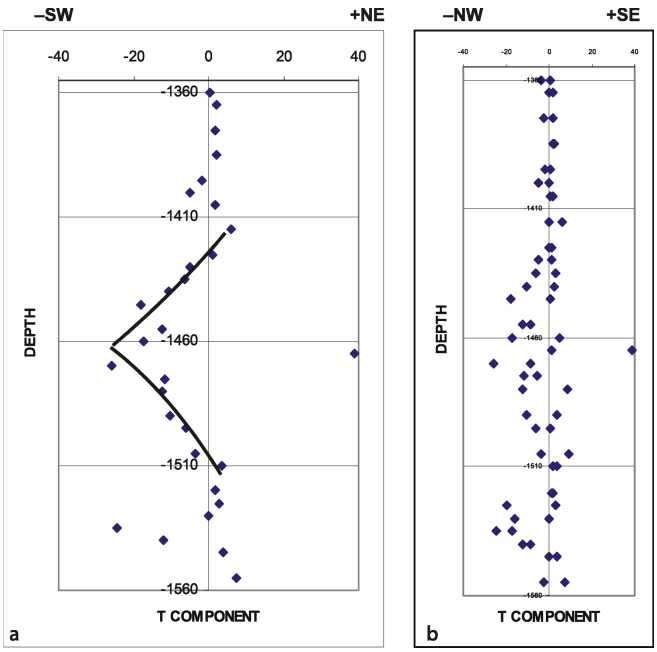

Fig. 9.25.
T and *L* component plots for data in Table 9.2, given $T = 052$ and $L = 322$. Plus and minus values assigned to the compass directions are for spreadsheet plotting purposes. **a** *T* component versus depth. **b** *L* component versus depth

9.7 Exercises

9.7.1 SCAT Analysis of the Sequatchie Anticline

Use the data in Table 9.1 to perform a complete SCAT analysis on the dip traverse across the Sequatchie anticline. Plot the azimuth-distance and the dip-distance diagrams. What are the *T* and *L* directions? What are the dip components in the *T* and *L* directions? Plot them on the dip-component diagrams.

9.7.2 SCAT Analysis of Bald Hill Structure

Use the data in Table 9.3 to perform a complete SCAT analysis on the dip traverse across the Bald Hill structure to see if a fault is present and its location and orientation, given that the faults in the area are reverse.

9.7.3 SCAT Analysis of Greasy Cove Anticline

Perform a complete SCAT analysis on the Greasy Cove anticline (Table 9.4). Consider both fold and fault geometry. The anticline is part of the southern Appalachian fold-thrust belt.

Table 9.3.
Bald Hill bedding attitudes

Distance from the northwest (km)	Attitude Dip, azimuth	T component	L component
0.54	60, 310		
0.70	90, 289		
0.90	55, 311		
1.10	40, 295		
1.30	14, 124		
2.38	12, 319		
2.68	26, 281		

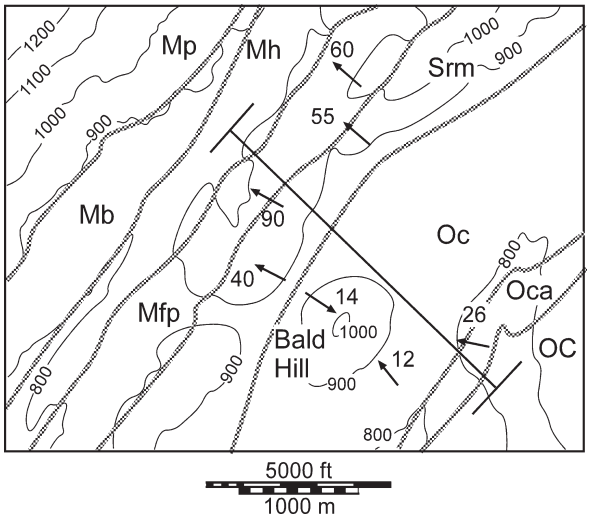

Fig. 9.26.
Geologic map of the Bald Hill area. Topographic contours (in feet) are *thin lines*; geologic contacts are *wide gray lines*. Data have been projected parallel to strike onto NW-SE traverse line. (Modified from Burchard and Andrews 1947)

Table 9.4.
Southeastern Greasy Cove anticline bedding attitudes

Distance (ft)	Bedding attitude	T component	L component
0	10, 300		
200	35, 302		
500	43, 293		
600	85, 300		
1 200	90, 329		
1 500	70, 130		
1 600	45, 133		
2 000	70, 133		
2 100	30, 130		
2 200	50, 130		
3 500	60, 133		
4 000	40, 150		